

Electrostatic quantum dot confinement in phosphorene

Bartłomiej Szafran

*AGH University of Science and Technology,
Faculty of Physics and Applied Computer Science,
al. Mickiewicza 30, 30-059 Kraków, Poland*

We consider states localized by electrostatic potentials in phosphorene using an atomistic tight binding approach. From the results of the tight-binding calculations of the confined states we extract effective masses for the conduction band electrons in the armchair and zigzag directions. The masses derived in this way are used for a simple single-band effective mass model which, as we find, reproduces very well the tight-binding energy spectrum in external magnetic field, the probability densities and the interaction effects. Both methods produce Wigner crystallization for the ground-state of the electron pair with the single-electron islands separated in the armchair direction already for small quantum dots.

I. INTRODUCTION

Black phosphorus (BP) is a layered semiconductor material that attracts a growing attention for its basic properties and possible applications [1–5]. BP with direct band gap [6] that falls within the visible range for few-layer systems [7–9] is investigated for optoelectronic applications [3]. Separation of few-layer material down to a monolayer (phosphorene) [10] is now routinely accomplished. The lateral confinement for optics is achieved in nanocrystals [11–17] quantum dots (QDs) that support confinement of both electrons and holes with by a mere finite size of the medium.

The growth of BP on nonmetallic substrates, its coating and gating allows for fabrication of field effect transistors [18] that recently reached a long-term air stability stage at room temperatures [19, 20]. The integer [21, 22] and fractional quantum Hall [23] effect, the latter being a fingerprint of strong correlations between interacting carriers, has already been reported [23]. The electrostatic QDs in bulk semiconductors [24], bilayer graphene [25] or carbon nanotubes [26] with their clean confinement independent of the details of the nanocrystal edges, allow for precise studies of localized states, energy spectra, coherence times [24] electron-electron interactions [27] control of the charge [28, 29] and spin [30] degrees of freedom. Although the advanced stage of BP field effect transistors has been reached [18–23] so far there are neither experimental nor theoretical literature on electrostatic QD confinement in BP. In this paper we study a single- and two-electrons confined in a phosphorene QD by an external potential that can be induced by electrostatic confinement.

The electrostatic confinement potential is usually parabolic near its minimum [31]. For materials with a parabolic dispersion relation the quantum harmonic oscillator is formed in this way, with the Fock-Darwin dependence on the external magnetic field for the isotropic case [27]. The anisotropy of phosphorene crystal structure [4] is translated to the in-plane anisotropy of the valence and conduction bands [1, 6, 32], with the effective masses

along the zigzag direction that are much larger than in the armchair direction [32]. The heavy masses provide stronger localization and may trigger strong interaction effects. The BP energy bands deviate from parabolic [33–35] near the conduction and valence band extrema. Due to the non-parabolicity a precise continuum description calls for $k \cdot p$ modelling of the low energy bands with the coupling between the conduction and valence bands [35–38]. The coupling is relatively weakest for monolayer BP due to the band gap that grows with reduction of the number of layers [7, 9]. In phosphorene the Landau levels are nearly linear on the external magnetic field and the non-linear corrections turn out to be small [39, 40]. On the other hand already for bilayer phosphorene the energy spectra in external magnetic field is very complex, non-linear and corresponding to different effective masses for each level [39]. The relatively simple form of Landau levels for phosphorene [39, 40] motivated us to look for description of the confined states in a parabolic single-band effective mass modeling that we compare to the atomistic tight-binding results. Although the tight-binding spectrum deviates from the exact quantum harmonic oscillator spectrum, the single and two-electron levels calculated by the tight-binding method can be surprisingly well reproduced by the simple single-band effective mass model including the magnetic field dependence, the form of the wave functions and electron-electron interaction effects.

II. THEORY

A. single-electron Hamiltonian

We consider a monolayer BP (see Fig. 1) with zigzag lines extended along the x direction and the armchair lines along the y axis. We use the effective tight-binding Hamiltonian of Ref. [41],

$$H_{TB} = \sum_{kl} t_{kl} p_{kl} c_k^\dagger c_l + \sum_k V_k c_k^\dagger c_k + \frac{g\mu_B B}{2} \sigma_z, \quad (1)$$

where the first sum describes the hopping between the neighbor atoms, and p_{kl} is the Peierls phase that introduces the orbital effects of the magnetic field $p_{kl} = e^{i \frac{e}{\hbar} \int_{r_k}^{r_l} \vec{A} \cdot d\vec{l}}$ to the hopping elements. We use the symmetric gauge $\mathbf{A} = (A_x, A_y, A_z) = (-By/2, Bx/2, 0)$ for the perpendicular magnetic field $(0, 0, B)$. The hopping integrals t_{kl} adopted from Ref. [41] and listed in Table I. The pairs of ions that correspond to the two largest values of t_{kl} are linked in Fig. 1 by blue ($t_{kl} = -1.486$ eV) and red ($t_{kl} = 3.729$ eV) lines. The second sum of Eq. (1) introduces the external potential, and the last term stands for the Zeeman effect with the Landé factor $g = 2$, and Bohr magneton μ_B . We consider states in a finite rectangular flake of phosphorene with a side length of 87 nm in the x direction and 44 nm in the y direction with over 100 thousand ions.

For the external potential we use the harmonic oscillator potential

$$V(x, y) = \frac{1}{2} m_x \omega^2 x^2 + \frac{1}{2} m_y \omega^2 y^2, \quad (2)$$

where $\hbar\omega$ is the oscillator energy, the m_x and m_y are the electron effective masses in the armchair and zigzag directions, respectively. For $m_x \neq m_y$ potential (2) is anisotropic. In Eq. (1) V_k is the potential on k th ion, $V_k = V(x_k, y_k)$, where x_k , and y_k are the coordinates of the k th ion. The actual band structure is not parabolic and the bands are flat near the conduction minimum so in the literature one finds a range of values for the effective mass. In this paper we establish m_x and m_y in the potential of Eq. (2) as fit parameters for the tight-binding spectrum to reproduce the harmonic oscillator spectrum at $B = 0$.

B. confined electron pair in the tight binding approach

We calculate the spectrum for a confined electron pair with the Hamiltonian,

$$H_{2e} = \sum_i d_i^\dagger d_i E_i + \frac{1}{2} \sum_{ijkl} d_i^\dagger d_j^\dagger d_k d_l V_{ijkl}, \quad (3)$$

where d_i^\dagger is the electron creation operator for the single-electron energy level E_i and the Coulomb matrix elements read

$$V_{ijkl} = \kappa \langle \psi_i(\mathbf{r}_1) \psi_j(\mathbf{r}_2) | \frac{1}{|\mathbf{r}_{12}|} | \psi_k(\mathbf{r}_1) \psi_l(\mathbf{r}_2) \rangle, \quad (4)$$

where $\kappa = e^2/(4\pi\epsilon\epsilon_0)$. We consider that the phosphorene is embedded in Al_2O_3 matrix and use its dielectric constant $\epsilon_0 = 9.1$. We integrate the Coulomb elements for the single-electron wave functions ψ spanned by the atomic orbitals $3p_z$ of P atoms,

$$\psi_i(\mathbf{r}_i) = \sum_k C_k^i p_z^k(\mathbf{r}_i), \quad (5)$$

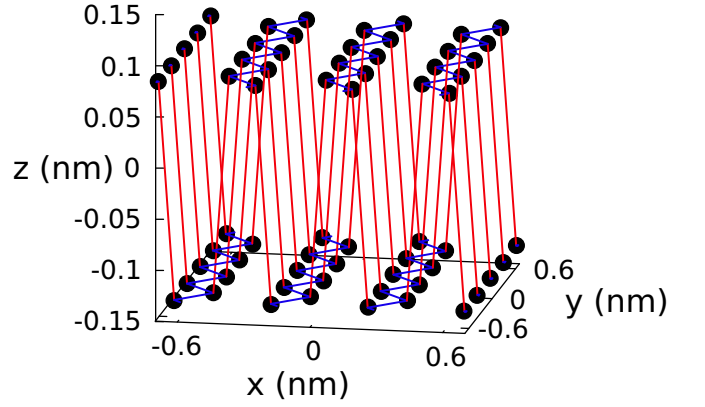


FIG. 1. Crystal structure of phosphorene with zigzag lines extended along the y direction. The zigzag bonds appear on two parallel planes shifted in the z direction. The links between the atoms show the pairs of the largest absolute values of the hopping energy (see Table I). The nearest neighbors within the zigzag chain are linked with the blue lines that are spaced by 2.22 \AA with the hopping energy of -1.486 eV. The red lines show the nearest-neighbor links between the zigzag chains of separate planes that are 2.24 \AA long with the hopping energy of 3.729 eV.

$$\begin{aligned} V_{ijkl} &= \kappa \langle \psi_i(\mathbf{r}_1) \psi_j(\mathbf{r}_2) | \frac{1}{|\mathbf{r}_{12}|} | \psi_k(\mathbf{r}_1) \psi_l(\mathbf{r}_2) \rangle \\ &= \kappa \sum_{\substack{a, \sigma_a; b, \sigma_b; \\ c, \sigma_c; d, \sigma_d}} C_{a, \sigma_a}^{i*} C_{b, \sigma_b}^{j*} C_{c, \sigma_c}^k C_{d, \sigma_d}^l \delta_{\sigma_a; \sigma_d} \delta_{\sigma_b; \sigma_c} \times \\ &\quad \langle p_z^a(\mathbf{r}_1) p_z^b(\mathbf{r}_2) | \frac{1}{|\mathbf{r}_{12}|} | p_z^c(\mathbf{r}_1) p_z^d(\mathbf{r}_2) \rangle. \end{aligned} \quad (6)$$

For the Coulomb integral we apply the two-center approximation [45] $\langle p_z^a(\mathbf{r}_1) p_z^b(\mathbf{r}_2) | \frac{1}{|\mathbf{r}_{12}|} | p_z^c(\mathbf{r}_1) p_z^d(\mathbf{r}_2) \rangle = \frac{1}{r_{ab}} \delta_{ac} \delta_{bd}$ for $a \neq b$. The on-site integral ($a = b$) is calculated with the $3p_z$ atomic orbitals, $p_z(\mathbf{r}) = Nz(1 - \frac{Zr}{6}) \exp(-Zr/3)$, where N is the normalization constant and Z is the effective screened P nucleus charge as seen by $3p_z$ electrons. The single-center integral can then be calculated analytically, $I_{a=b} = \frac{3577}{46080} Z$ in atomic units. The Slater screening rules for $3p$ electrons in P atoms produce $Z = 4.8$, then $I_{a=b} = 10.14$ eV.

The Hamiltonian (3) is diagonalized with the configuration interaction approach in the basis of up to ~ 1000 two-electron Slater determinants constructed from the lowest-energy eigenfunctions of the single-electron Hamiltonian (1) of the conduction band.

C. single-band effective mass Hamiltonian

For description of the system in the effective mass Hamiltonian we take the single-band approximation with

$r_{kl}(\text{\AA})$	2.22	2.24	3.31	3.34	3.47
$t_{kl}(\text{eV})$	-1.486	3.729	-0.252	-0.071	-0.019
$r_{kl}(\text{\AA})$	4.24	4.37	5.18	5.38	5.49
$t_{kl}(\text{eV})$	0.186	-0.063	0.101	-0.042	0.073

TABLE I. Hopping parameters for the effective tight-binding model of Ref. [41]. The value of the hopping parameter t_{ij} is given below the distance between the corresponding P ions r_{ij} .

the Hamiltonian,

$$H_{em} = \frac{\left(-i\hbar\frac{\partial}{\partial x} + eA_x\right)^2}{2m_x} + \frac{\left(-i\hbar\frac{\partial}{\partial y} + eA_y\right)^2}{2m_y} + V(x, y) + \frac{g\mu_B B}{2}\sigma_z. \quad (7)$$

To diagonalize Hamiltonian we employ the finite difference method with the gauge-invariant discretization of Ref. [46] with the Peierls phases that account for the orbital effects of the magnetic field. For the mesh spacing Δx in both x and y directions the finite difference Hamiltonian defined by its action on the wave function $\Psi_{\mu,\nu} = \Psi(x_\mu, x_\nu) = \Psi(\mu\Delta x, \nu\Delta x)$,

$$H_{fd}\Psi_{\mu,\nu} \equiv \frac{\hbar^2}{2m_x\Delta x^2} (2\Psi_{\mu,\nu} - C_y\Psi_{\mu,\nu-1} - C_y^*\Psi_{\mu,\nu+1}) + \frac{\hbar^2}{2m_y\Delta x^2} (2\Psi_{\mu,\nu} - C_x\Psi_{\mu-1,\nu} - C_x^*\Psi_{\mu+1,\nu}) + V_{\mu,\nu}\Psi_{\mu,\nu}, \quad (8)$$

with $C_x = \exp(-i\frac{e}{\hbar}\Delta x A_x)$ and $C_y = \exp(-i\frac{e}{\hbar}\Delta x A_y)$.

With the eigenstates of Hamiltonian (7) obtained with the Hamiltonian given by Eq. (8) we calculated the two-electron spectrum in the manner discussed above for the tight-binding method. The only difference is the on-site integral which is evaluated numerically

$$I_{a=b} = \frac{\int_{-\Delta x/2}^{\Delta x/2} dx_1 \int_{-\Delta x/2}^{\Delta x/2} dy_1 \int_{-\Delta x/2}^{\Delta x/2} dx_2 \int_{-\Delta x/2}^{\Delta x/2} dy_2}{\sqrt{(x_1 - x_2)^2 + (y_1 - y_2)^2}} \quad (9)$$

with the Monte Carlo method. With the finite difference mesh we cover the same area as in the tight-binding approach and use $\Delta x = 0.2$ nm.

III. RESULTS

As stated at the end of Section II.A we look for the effective masses by a fit of the tight binding spectrum obtained for Hamiltonian (1) to the harmonic oscillator spectrum with potential (2). At $B = 0$ the harmonic oscillator the n th excited energy level is $n+1$ fold degenerate (spin excluded) with the energy $n\hbar\omega$ above the ground

$n\hbar\omega$	ΔE_{TB} (meV)			
10	9.83	10.04		
20	19.77	19.93	20.08	
30	29.69	29.79	30.16	30.36
40	39.63	39.64	40.17	40.50 41.00

TABLE II. The energy above the ground state obtained for lowest 14 excited states with the tight-binding method for confinement potential given by Eq. (2), $m_x = 0.172m_0$, $m_y = 3.576m_0$ and $\hbar\omega = 10$ meV in the absence of external magnetic field. In the subsequent rows we group the nearly degenerate energy levels that for the quantum harmonic oscillator should be placed exactly at the energy of $n\hbar\omega$ above the ground state with $n = 1, 2, 3$ and 4.

n	S/T	ΔE_{TB} (meV)	ΔE_{EM} (meV)
1	S	0	0
2	T	0.471	0.441
3	T	8.791	8.971
4	S	9.802	9.997
5	S	9.872	10.035
6	S	10.103	10.056
7	T	10.276	10.424
8	T	10.599	10.517
9	S	16.628	16.662

TABLE III. The energy spacings in meV from the ground-state as calculated with the tight binding method (ΔE_{TB}) and with the effective mass approximation (ΔE_{EM}) for potential of Eq. 2 at $B = 0$.

state. For the fit we took $\hbar\omega = 10$ meV and considered 15 lowest energy levels obtained with the tight-binding approach, including the ground-state. The fitness function was taken in form of sum of squares of the energy difference between energy levels obtained with the tight-binding approach and the corresponding quantum harmonic oscillator energy levels. The best fit was obtained for $m_x = 0.172m_0$ and $m_y = 3.576m_0$, with the energies that fall within the range of the values indicated in the literature, e.g., $m_x/m_0 = 0.148$ [42], 0.16 [43], 0.17 [32], 0.2 [44], and $m_y/m_0 = 1.12$ [32], 1.237 [42], 1.24 [43], 6.2 [7] or 6.89 [44]. The optimal spacings between the excited states and the ground states are given in Table II. The degeneracy of the excited energy levels can only be approximate. The largest deviations of the energy levels of the degenerate groups with $n = 1, 2, 3, 4$ from the harmonic oscillator spectrum energies are: 0.17 meV, 0.23 meV, 0.36 meV, and 1 meV, respectively.

The dependence of the single-electron energy levels in the external magnetic field is given in Fig. 2 with the same scale applied for the vertical and horizontal axis. The lifted degeneracy of the higher energy levels at $B = 0$ is evident in the tight-binding model Fig. 2(a). Nevertheless, the magnetic field dependence of the tight-binding spectrum is in a quite good agreement with the results of

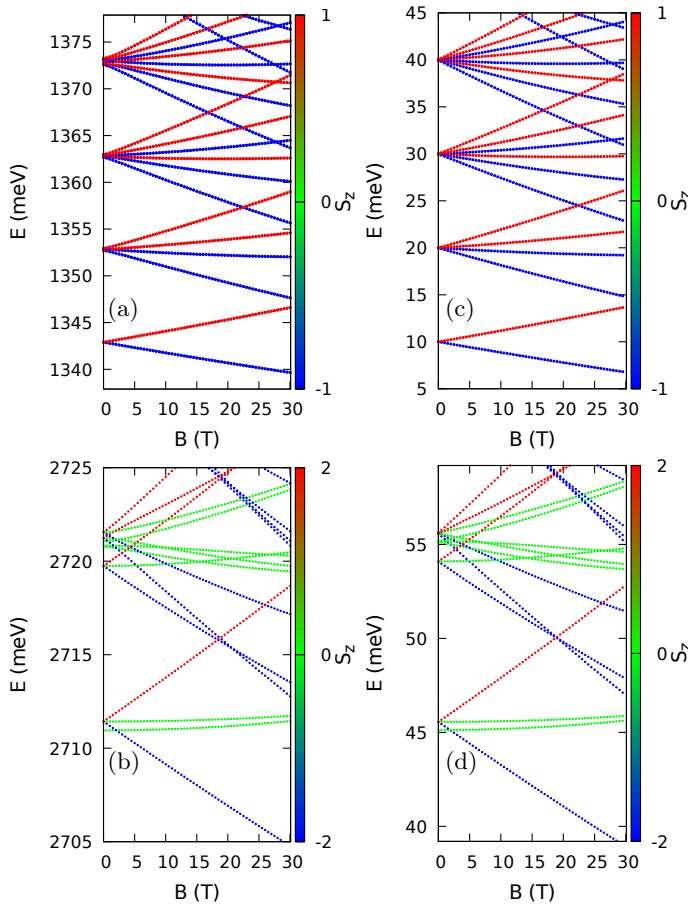


FIG. 2. Tight-binding (a,b) spectrum and the results of the single-band effective mass approximation (c,d) for a single (a,c) and two electrons (b,d) confined in potential (2) with $m_x = 0.172m_0$, $m_y = 3.576m_0$ and $\hbar\omega = 10$ meV in the external magnetic field. The color of the line indicates the z - component of the spin.

the effective mass approximation. The probability density calculated with the tight-binding approach for the spin-down states: the ground state, the first and the second excited states are displayed in Fig. 3(a,c) and (e), respectively. For comparison the probability densities calculated with the effective mass approximation are given in Fig. 3(b,d,f). The probability densities for these low-energy states are elongated along the armchair (x) direction and more strongly localized in the zigzag direction (y) and are very similar for the tight binding Hamiltonian and in the single-band approximation.

The energy spectra for the electron pair are plotted in Fig. 2(b,d). A more detailed comparison is given in Table III where the spacing from the ground state is given along with the information whether the state is spin singlet or spin triplet. The singlet-triplet order of the energy levels is very well reproduced by the effective mass approximation and the energy spacings as calculated by the continuum method agree with a precision

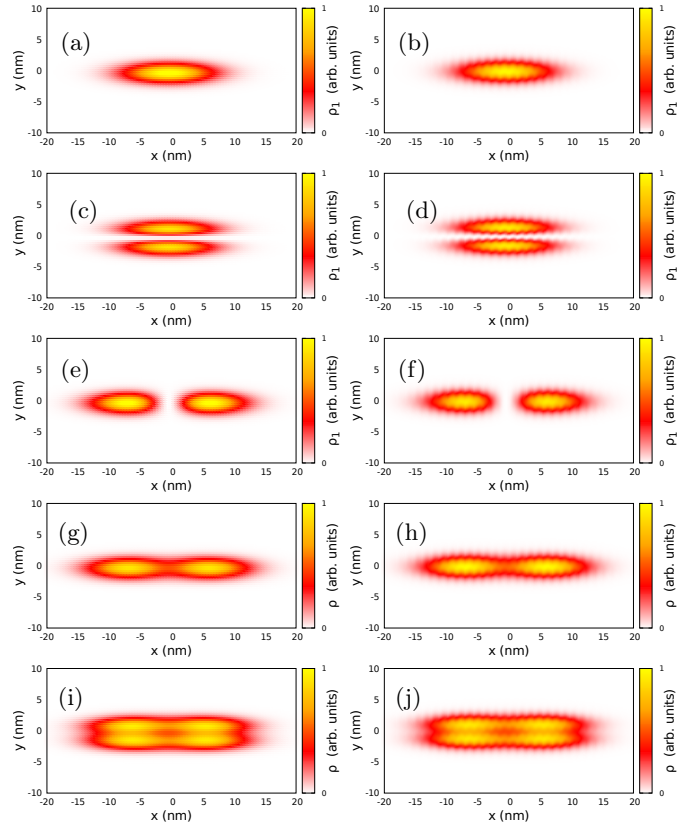


FIG. 3. Probability density for the single-electron (a-f) and two-electron (g-j) states calculated with the tight-binding – left column – (a,c,e,g,i) and effective mass approximation – right column (b,d,f,h,j). Panels (a,b) correspond to the single-electron ground state, and (g,h) to the two-electron ground state. Second (c,d) and third row (e,f) of plots correspond to the first and second excited single-electron states. The last row (i,j) show the probability density for the second excited triplet that corresponds to $n = 3$ in Table III.

of about 0.2 meV to the tight-binding results. In Fig. 3(g,h) we compare the results for the ground-state two-electron density as obtained with the tight-binding [Fig. 3(g)] and the continuum approach [Fig. 3(h)]. Due to the large mass in the zigzag direction the states are localized near the $y = 0$ line, to a quasi-one dimensional channel that promotes the separation of single-electron charges, i.e. Wigner crystallization, along the x axis. In the first excited triplet the separation of charges is similar albeit slightly more pronounced (not shown). The results for the second excited triplet are given in Fig. 3(i,j). In this state four local maxima of the charge density appear instead of the two single-electron islands found in the ground state. Results of both tight-binding [Fig. 3(i)] and effective mass approaches [Fig. 3(j)] are again very similar.

In order to compare the results of both methods for nonparabolic potential we introduced a perturbation to potential given by Eq. (2) introducing a repulsive Gaus-

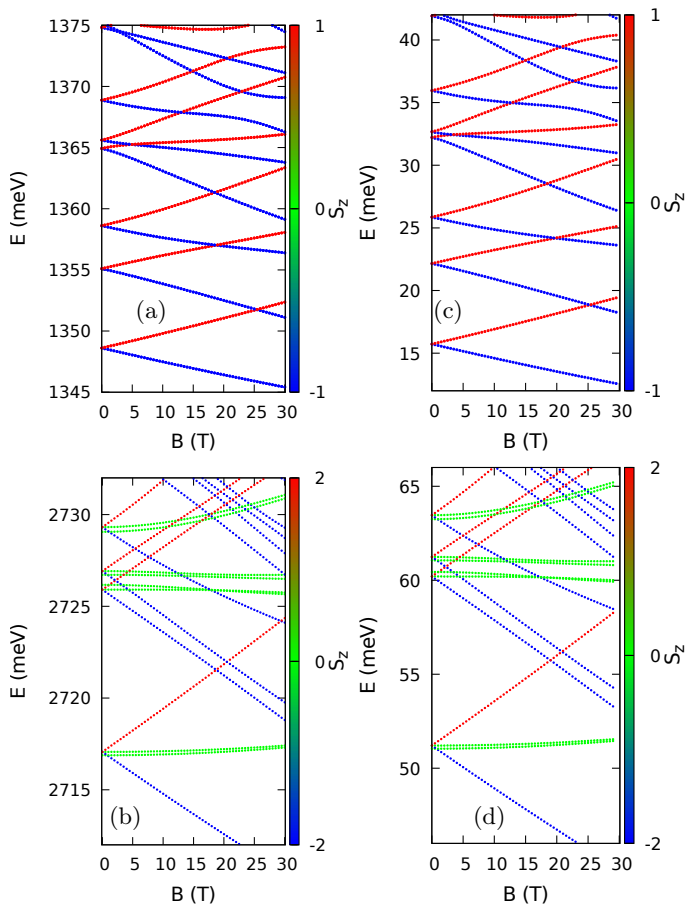


FIG. 4. Same as Fig. 2 but for a Gaussian perturbation to the parabolic potential given by Eq. (10).

sian centered at the y axis, i.e. for potential

$$V_p(x, y) = V(x, y) + V_z \exp\left(-\frac{(y - y_s)^2 + x^2}{R^2}\right), \quad (10)$$

where $V(x, y)$ is given by Eq. (2), $V_z = 30$ meV and $y_s = R = 5$ nm. Comparison of the spectra is given in Fig. 4 for the single electron Fig. 4(a,c) and for the electron pair Fig. 4(b,d). For the single-electron we notice that the perturbation lowers the symmetry of the potential and reduces the degeneracy found for $B = 0$. The energy levels enter into avoided crossings that replace the crossings of the high-symmetry case of Fig. 2(a,b). For the electron pair we find that the perturbation enhances the separation of the charges for the electron pair which leads to a reduced triplet-singlet energy difference in the ground-state. The Wigner localization in quasi one-dimensional systems is accompanied by the singlet-triplet degeneracy [47]. Overall agreement between the results is very well also for nonparabolic external potential.

IV. SUMMARY AND CONCLUSIONS

We have determined the energy spectra of single electron and electron pair in a parabolic external potential using the effective tight-binding Hamiltonian for phosphorene, including the effects of the external magnetic field and the electron-electron interaction. We determined the effective masses for which the lowest energy levels as calculated with the tight-binding approach approximately reproduce the exact quantum harmonic oscillator spectrum. The fitted masses were then used for a simple single-band effective mass model for the conduction band electrons. The model reproduces quite well the results of the tight-binding method in the external magnetic field. The Wigner crystallization of the two-electron ground-state is found at $B = 0$ already for a relatively large oscillator energy of 10 meV and small quantum dot size. For the two-electrons the effective mass model correctly reproduces the sequence of the singlet and triplet energy levels and the interaction effects. The present demonstration that the states confined by electrostatic potentials in phosphorene can be with a good approximation described within the simple single-band effective mass model opens perspectives for analytical and semi-analytical treatment of the electrostatic quantum dots in monolayer black phosphorus.

-
- [1] F. Xia, H. Wang, and Y. Jia, *Rediscovering black phosphorus as an anisotropic layered material for optoelectronics and electronic*, Nat. Commun. **5**, 4458 (2014).
 - [2] A. Castellanos-Gomez, L. Vicarelli, E. Prada, J.O. Island, K.L. Narasimha-Acharya, S.I Blanter, D.J. Groenendijk, M. Buscema, G.A. Steele, J.V. Alvarez, H.W. Zandbergen, J.J. Palacios, and H.S.J. van der Zant *Isolation and characterization of few-layer black phosphorus*, 2D Materials **1**, 025001 (2014).
 - [3] J. Miao, L. Zhang, and C. Wang, *Black phosphorus electronic and optoelectronic devices*, 2D Materials **6**, 032003 (2019).
 - [4] M. Akhar et al, G. Anderson, R.Zhao, A. Alruqi, J.E. Mroczkowska, G. Sumanasekera, J.B. Jasinski, *Recent advances in synthesis, properties, and applications of phosphorene*, npj 2D Mater Appl **1**, 5 (2017).
 - [5] S. Fukuoka, T. Taen, and T. Osada, *Electronic Structure and the Properties of Phosphorene and Few-Layer Black Phosphorus*, J. Phys. Soc. Jpn. **84**, 121004 (2015).
 - [6] R. Schuster, J. Trinckauf, C. Habenicht, M. Knupfer, and B. Büchner, *Anisotropic Particle-Hole Excitations in Black Phosphorus*, Phys. Rev. Lett. **115**, 026404 (2015).
 - [7] V. Tran, R. Soklaski, Y. Liand, and L. Yang, *Layer-controlled band gap and anisotropic excitons in few-layer black phosphorus*, Phys. Rev. B **89**, 235319 (2014).
 - [8] N. Ehlen, B. V. Senkovskiy, A. V. Fedorov, A. Perucchi, P. Di Pietro, A. Sanna, G. Profeta, L. Petaccia, and A. Grüneis, *Evolution of electronic structure of few-layer phosphorene from angle-resolved photoemis-*

- sion spectroscopy of black phosphorus, *Phys. Rev. B* **94**, 245410 (2016).
- [9] L. Seixas, A. S. Rodin, A. Carvalho, and A. H. Castro Neto, *Exciton binding energies and luminescence of phosphorene under pressure*, *Phys. Rev. B* **91**, 115437 (2015).
- [10] H. Liu, A.T. Neal, Z.Zhu, Z. Luo, X. Xu, D. Tomanek, and P.D. Ye, *Phosphorene: An Unexplored 2D Semiconductor with a High Hole Mobility*, *ACS Nano* **8**, 4033 (2014).
- [11] M. Lee, Y.H. Park, E.B. Kang, A. Chae, Y. Choi, S. Jo, Y.J. Kim, S.J. Park, B. Min, T.K. An, J. Lee, S.I. In, S.Y. Kim, S.Y. Park, I. In, *Highly Efficient Visible Blue-Emitting Black Phosphorus Quantum Dot: Mussel-Inspired Surface Functionalization for Bioapplication*, *ACS Omega* **2**, 7096 (2017).
- [12] Z. Sun, H. Xie, S. Tang, Y. Xue-Fang, G.Zhinan, J. Shao, H. Zhang, H. Huang, H. Wang, and P.K. Chu, *Ultrasmall Black Phosphorus Quantum Dots: Synthesis and Use as Photothermal Agents*, *Angewandte Chemie* **127**, 11688 (2015).
- [13] M. Wang, Y. Liang, Y. Liu, G. Ren, Z. Zhang, S. Wu, and J. Shen, *Ultrasmall black phosphorus quantum dots: synthesis, characterization, and application in cancer treatment*, *Analyst* **143**, 5822 (2018).
- [14] R. Gui, H. Jin, Z. Wang, and J. Li, *Black phosphorus quantum dots: synthesis, properties, functionalized modification and applications*, *Chem. Soc. Rev.* **47**, 6795 (2018).
- [15] V. A. Saroka, I. Lukyanchuk, M. E. Portnoi, and H. Abdelsalam, *Electro-optical properties of phosphorene quantum dots*, *Phys. Rev. B* **96**, 085436 (2017).
- [16] H. Abdelsalam, V.A. Saroka, I. Lukyanchuk, and M.E. Portnoi, *Multilayer phosphorene quantum dots in an electric field: Energy levels and optical absorption*, *J. App. Phys.* **124**, 124303 (2018).
- [17] F. X. Liang, Y. H. Ren, X. D. Zhang, and Z. T. Jiang, *Electronic properties and optical absorption of a phosphorene quantum dot*, *J. App. Phys.* **123**, 125109 (2018).
- [18] L. Li, Y. Yu, Q. Ge, X.Ou, H. Wu, D. Feng, X.H. Chen, and Y. Zhang, *Black phosphorus field-effect transistors.*, *Nat. Nanotechnol.* **9**, 372 (2014).
- [19] D. He, Y. Wang, Y. Huang, Y. Shi, X. Wang, and X. Duan, *High-Performance Black Phosphorus Field-Effect Transistors with Long-Term Air Stability*, *Nano Lett.* **19**, 331 (2019).
- [20] X.Li, Z. Yu, X. Xiong, T. Li, T. Gao, R. Wang, R. Huang, and Yanqing Wu, *High-speed black phosphorus field-effect transistors approaching ballistic limit*, *Sci. Adv.* **5** eaau3194 (2019).
- [21] G. Long, D. Maryenko, J. Shen, S. Xu, J. Hou, Z. Wu, W.K. Wong, T. Han, J. Lin, Y. Cai, R. Lortz, and N. Wang, *Achieving Ultrahigh Carrier Mobility in Two-Dimensional Hole Gas of Black Phosphorus*, *Nano Lett.* **16**, 7768 (2016).
- [22] G. Long, D. Maryenko, S. Pezzini, S. Xu, Z. Wu, T. Han, J. Lin, C. Cheng, Y. Cai, U. Zeitler, and N. Wang *Ambipolar quantum transport in few-layer black phosphorus*, *Phys. Rev. B* **96**, 155448 (2017).
- [23] J. Yang et al., *Integer and Fractional Quantum Hall effect in Ultrahigh Quality Few-layer Black Phosphorus Transistors*, *Nano Lett.* **18**, 229 (2018).
- [24] R. Hanson, L. P. Kouwenhoven, J. R. Petta, S. Tarucha, and L. M. K. Vandersypen, *Spins in few-electron quantum dots*, *Rev. Mod. Phys.* **79**, 1217 (2007).
- [25] M. Eich, R. Pisoni, H. Overweg, A. Kurzman, Y. Lee, P. Rickhaus, T. Ihn, K. Ensslin, F. Herman, M. Sigrist, K. Watanabe, and T. Taniguchi, *Spin and Valley States in Gate-Defined Bilayer Graphene Quantum Dots*, *Phys. Rev. X* **8**, 031023 (2018).
- [26] E.A. Laird, F. Kuemmeth, G.A. Steele, K. Grove-Rasmussen, J. Nygaard, K. Flensberg, and Leo P. Kouwenhoven, *Quantum transport in carbon nanotubes*, *Rev. Mod. Phys.* **87**, 703 (2015).
- [27] S. Reimann and M. Manninen, *Electronic structure of quantum dots*, *Rev. Mod. Phys.* **74**, 1283 (2002).
- [28] J. Gorman, D. G. Hasko, and D. A. Williams, *Charge-Qubit Operation of an Isolated Double Quantum Dot*, *Phys. Rev. Lett.* **95**, 090502 (2005).
- [29] K. D. Petersson, J. R. Petta, H. Lu, and A. C. Gossard *Phys. Rev. Lett.* **105**, *Quantum Coherence in a One-Electron Semiconductor Charge Qubit*, 246804 (2010).
- [30] D. D. Awschalom, L. C. Bassett, A. S. Dzurak, E. L. Hu, and J. R. Petta, *Quantum Spintronics: Engineering and Manipulating Atom-Like Spins in Semiconductors*, *Science* **339**, 1174 (2013).
- [31] S.Bednarek, B.Szafran, K. Lis, J.Adamowski, *Modeling of electronic properties of electrostatic quantum dots*, *Phys. Rev. B* **68**, 155333 (2003).
- [32] J. Qiao, X. Kong, Z.X. Hu, F. Yang, W. Ji, *High-mobility transport anisotropy and linear dichroism in few-layer black phosphorus*, *Nat. Commun.* **5**, 4475 (2014).
- [33] P. Li, *Origin of the electromagnetic anisotropy in monolayer black phosphorus*, *Phys. Rev. B* **100**, 205418 (2019).
- [34] P. Li and I. Appelbaum, *Electrons and holes in phosphorene*, *Phys. Rev. B* **90**, 115439 (2014).
- [35] A. S. Rodin, A. Carvalho, and A. H. Castro Neto, *Strain-Induced Gap Modification in Black Phosphorus*, *Phys. Rev. Lett.* **112**, 176801 (2014).
- [36] T. Low, A. S. Rodin, A. Carvalho, Y. Jiang, H. Wang, F. Xia, and A. H. Castro Neto, *Tunable optical properties of multilayer black phosphorus thin films*, *Phys. Rev. B* **90**, 075434 (2014).
- [37] T. Low, R. Roldan, H. Wang, F. Xia, P. Avouris, L. M. Moreno, and F. Guinea, *Plasmons and Screening in Monolayer and Multilayer Black Phosphorus*, *Phys. Rev. Lett.* **113**, 106802 (2014).
- [38] L. C. Low Yan Voon, A. Lopez-Bezanilla, J. Wang, Y. Zhang, and M. Willatzen, *Effective Hamiltonians for phosphorene and silicene*, *New J. Phys.* **17**, 025004 (2015).
- [39] J. M. Pereira, Jr. and M. I. Katsnelson, *Landau levels of single-layer and bilayer phosphorene*, *Phys. Rev. B* **92**, 075437 (2015).
- [40] X. Zhou, R. Zhang, J.P. Sun, Y.L. Zou, D. Zhang, W.K. Lou, F. Cheng, G.H. Zhou, F. Zhai, and K. Chang, *Landau levels and magneto-transport property of monolayer phosphorene*, *Sci. Rep.* **5**, 12295 (2015).
- [41] A. N. Rudenko, S. Yuan and M. I. Katsnelson, *Toward a realistic description of multilayer black phosphorus: From GW approximation to large-scale tight-binding simulations*, *Phys. Rev. B* **92**, 085419(R) (2015).
- [42] B.Sa, Y.-L. Li, Z. Sun, J. Qi, C. Wen, and B. Wu, *The electronic origin of shear-induced direct to indirect gap transition and anisotropy diminution in phosphorene*, *Nanotechnology* **26** 215205 (2015).
- [43] X. Peng, Q. Wei, and A. Coppole, *Strain-engineered direct-indirect band gap transition and its mechanism in two-dimensional phosphorene*, *Phys. Rev. B* **90**, 085402

- (2014).
- [44] M. Van der Donck and F. M. Peeters, *Excitonic complexes in anisotropic atomically thin two-dimensional materials: Black phosphorus and TiS* , Phys. Rev. B **98**, 235401 (2018).
- [45] K.A. Guerrero-Becerra and M. Rontani, *Wigner localization in a graphene quantum dot with a mass gap*, Phys. Rev. B **90**, 125446 (2014).
- [46] M. Governale and C. Ungarelli, *Gauge-invariant grid discretization of the Schroedinger equation*, Phys. Rev. B **58**, 7816 (1998).
- [47] B. Szafran, F. M. Peeters, S. Bednarek, T. Chwiej, and J. Adamowski, *Spatial ordering of charge and spin in quasi-one-dimensional Wigner molecules*, Phys. Rev. B **70**, 035401 (2004).